Trajectory Optimization for a Low Cost Lunar Technology Demonstrator Mission

C. M. Fromm and C. Schmierer and A. Herbertz
German Aerospace Center (DLR)
74239 Hardthausen, Germany

Abstract

The high Δv (velocity increment) requirement for lunar missions (ca. 4000 m/s for a Hohmann transfer from low Earth orbit to low lunar orbit) necessitates a large total vehicle mass of a chemically propelled spacecraft, which is prohibitive for low cost missions. To enable low cost lunar missions highly efficient propulsion is required to minimize the total system mass and the associated cost of the transport from Earth to orbit. Therefore currently only electric propulsion seems feasible for such a mission. Electric propulsion, while allowing a high specific impulse, is associated with low thrust, which results in long transfer times, as implemented by the *SMART-1* probe (transfer time from Earth to Moon orbit of more than a year). One obstacle on the way to the moon is the Van-Allen radiation belt. It is important for the probe to minimize the exposure time in the most energetic parts of the radiation belt. The paper defines and discusses a lunar mission. Vehicle and propulsion system sizing are performed. High level cost assumptions are discussed. The transfer trajectory is optimized with respect to flight duration.

1. Introduction

In the 60s and 70s of the past century many robotic and manned missions have been flown to the moon by the United States and the Soviet Union. Since the turn of the century renewed interest in the moon has led to several lunar missions by many space faring nations. Among them the European technology demonstrator *SMART-1*, some orbital surveyors from the United States, missions from India, Japan and until now three Chinese missions, including a lander. For the near future several landers and some sample return missions are planned by various nations. An economically reasonable approach for a future European mission would be to combine technology demonstration with scientific objectives.

Although heavy lift transportation may offer better specific cost, a small launcher is likely to be the ideal choice to keep the total cost of such a demonstrator mission within an affordable budget. The moon is on the one hand so far away from Earth, as to require a significant velocity increment. On the other hand it is close enough to be reached under low thrust within reasonable time frames. Therefore solar electric propulsion (SEP) seems an optimum choice, when looking at a restricted mass budget, as imposed by the utilization of a small launcher.

The paper discusses methods used for optimization of a low thrust lunar trajectory. Some sample cases for lunar missions are evaluated and discussed.

2. Vehicle definition

To design the mission for technology demonstration, a robotic moon lander is suggested, which could also include a rover and/or a sample return vehicle. One major goal of scientific missions to the moon's surface is the analysis of the soil. For future missions like permanently maintained manned bases or in-situ resource utilization (ISRU), e.g. rocket fuel production, knowledge about the exact local composition of the soil is crucial for deciding on a landing area. The vehicle can be designed with the following modules:

- Orbiting module with electric propulsion system, power supply and possible communications relay
- Landing module with a storable propellants propulsion system, power supply and instrumentation for automated landing

- Optional rover to gather soil samples from multiple locations
- Either a sample return module or a field laboratory to analyze the samples locally

2.1 In-space propulsion

The propulsion system consists of thruster(s), power supply and propellants. The mass and performance data of the subsystems is based on published data of existing systems. Application of the listed or similar systems is assumed.

2.1.1 Main propulsion thrusters

For the main propulsion ion engines are assumed. The engine performance data used for calculations is listed in table 1.

Table 1: Propulsion characteristics

Engine type		RIT-22
Thrust	F	200 mN
Power	P_{prop}	7000 W
Specific impulse	I_{sp}	4200 s
Mass	m_{engine}	8.8 kg

2.1.2 Orbital maneuvering

For emergency purposes and attitude control a conventional reaction control system (RCS) is assumed.

2.1.3 Power supply

No power storage (i.e. batteries) is assumed for the in-space propulsion. As discussed later in section 3.2.1, the trajectory calculation assumes no thruster operation during shadow transits. The largely reduced power, which is delivered by the solar panels in the penumbra, will therefore be fully available for the on-board electronics. The payload's power storage will also be available during transit for any on going consumers, which may require power above which is supplied by the solar panels. Table 2 lists assumed characteristics for the solar panels, based on commercially available solar cells [12].

Table 2: Solar panel characteristics

Material		GaInP2/GaAs/Ge
Efficiency	η_{panel}	29.5%
Area mass		0.84 kg/m^2
Cover glass density	ρ_{glass}	2500 kg/m^3
Cover glass thickness	s_{glass}	0.335 mm

For the passage through the radiation belts, and the associated degradation of the solar panels, a power reserve of $\xi_{\text{power}} = 10\%$ is assumed. A typical angle of incidence efficiency (resulting from non vertical alignment of the solar panel area to the sun), of $\eta_\theta = 50\%$ is assumed. The required area A_{panel} of the solar panels can thus be calculated according to equation (1), based on the number of thrusters N, the solar constant at Earth distance ($E_0 = 1367$ W/m^2), and the normalized distance from the sun Z (i.e. distance measured in astronomical units (AUs)). Given the cover glass thickness, the total mass of the panel can be calculated, resulting in a specific power of 120 W/kg at beginning of life (BOL).

$$A_{\text{panel}} = \frac{N\, P_{\text{prop}}\, (1 + \xi_{\text{power}})\, Z^2}{E_0\, \eta_{\text{panel}}\, \eta_\theta} \tag{1}$$

2.1.4 Propellants

The fuel used for propulsion is xenon. A propellants reserve of $\xi_{\text{prop}} = 5\%$ is assumed.

Tank The tank is calculated as a single spherical tank for pressurized propellant. A volume efficiency of $\eta_{\text{vol}} = 95\%$ is assumed, meaning 95% of the tank volume is usable for propellant storage. Table 3 lists the tank's main characteristics. The pressure vessel mass is calculated according to equation (2). The total mass of the tank, including flanges, sensors, tank bladder etc. is assumed to be twice that value.

Table 3: Propellant tank characteristics

Propellant		Xenon
Initial pressure	p_{prop}	12 MPa
Initial temperature	T_{prop}	298.15 K
Propellant density	ρ_{prop}	1884.9 kg/m^3
Tank wall material		TiAlV4
Wall material allowable stress	σ_{tank}	1070 MPa
Wall material density	ρ_{tank}	4450 kg/m^3
Margin of safety	S	2

$$m_{\text{pressure-vessel}} = \frac{3}{2} \frac{S\ (1 + \xi_{\text{res}})}{\eta_{\text{vol}}} \left[\frac{p\ m}{\rho}\right]_{\text{prop}} \left[\frac{\rho}{\sigma}\right]_{\text{tank}} \tag{2}$$

Valves For the mass estimation, the mass of the valves is based on the commercially available Xenon Regulator Feed System (XRFS) [4], adding a small margin.

2.2 Lander Design

The initial mass of the lander is limited by the maximum mass that can be transferred into a moon orbit with a certain launcher and electric propulsion system. The lander itself is in need of a chemical propulsion system since the landing and ascent on the moon needs high thrust and throttle-ability. It is supposable to use a liquid propulsion system using classical storable propellants like hydrazine (N_2H_4) and nitrogen tetroxide (N_2O_4) or green propellants, which replace those. Another possibility is the use of hybrid propulsion systems with solid fuel and liquid oxidizer. All of those options will have a similar specific impulse. The Δv for the de-orbit burn, the descent to the lunar surface and also the ascent and moon escape and Earth reentry for the lander and sample return mission, can be calculated ideally using Hohmann-transfers. Table 4 provides an overview over typical velocity increments for a lunar sample return mission. A detailed analysis of moon landing and sample return trajectories is on-going to optimize the vehicle design and the thrust phases for such a mission regarding different kind of propulsion system options.

Table 4: Ideal Δv of a lunar landing and sample return mission

Phase	**Initial orbit**	**Final orbit**	**Center body**	**Ideal Δv**
De-orbit burn	1000 km circular orbit	1000 x 0 km orbit	Moon	159 m/s
Descent & landing	1000 km x 0 km orbit	landed on surface	Moon	1858 m/s
Ascent	landed on surface	1000 km x 0 km orbit	Moon	1858 m/s
Circularization	1000 km x 0 km orbit	1000 km circular orbit	Moon	159 m/s
Moon escape	1000 km circular orbit	parabolic trajectory	Moon	550 m/s
Earth reentry	405500 km x 363300 km orbit	405500 km x 45 km orbit	Earth	570 m/s

2.3 Rover or Sample Return

If the total mass of the spacecraft, which can be transferred to a moon orbit, by the chosen launcher and the SEP transfer vehicle, is high enough, both a rover for gathering samples and a sample return module can be included in the mission design. If the limit of the lunar payload mass is low, the design has to be adjusted to allow achieving of the most important scientific goals. First the number and total mass of the samples returned to Earth can be reduced, then the rover can be discarded from the mission design and instead a robotic arm can gather samples adjacent to the landing vehicle. Another option is to replace the sample return with an in-situ analysis of the samples directly at the landing site. The advantage of sample return is however, that much more analyses can be done, with more complex instruments. Also the samples can be stored for potential future analyses.

3. Trajectory simulation

The methods used in the calculations presented in this paper are described in more detail in a parallel publication [5].

3.1 Orbital elements and perturbations

The orbit of a satellite can be described by six Keplerian elements, the semi-major axis, a, the eccentricity, e, the inclination, i, the right ascension of the ascending node, Ω, the argument of perigee, ω, and the true anomaly, θ. The latter is used to determine the position of the satellite within the orbit. Assuming a perfect spherical Earth and under the absence of perturbing forces, the orbit would be closed and fixed in space, i.e., no variation in the orbital elements, a, e, i, Ω and ω.

3.1.1 Perturbation Theory

As mentioned earlier, any perturbation acting on a satellite leads to a variation of its orbital elements. In this study the Gauss variational equations are used for the calculation of the perturbed orbital elements.

$$\frac{da}{dt} = \frac{2a^2}{h}\left(e\sin\theta a_\mathrm{r} + pr^{-1}a_\mathrm{t}\right) \tag{3}$$

$$\frac{de}{dt} = h^{-1}\left(p\sin\theta a_\mathrm{r} + \left(\left[p+r\right]\cos\theta + re\right)a_\mathrm{t}\right) \tag{4}$$

$$\frac{di}{dt} = h^{-1}r\cos\left(\omega+\theta\right)a_\mathrm{n} \tag{5}$$

$$\frac{d\Omega}{dt} = \frac{r\sin\left(\omega+\theta\right)}{h\sin i}a_\mathrm{n} \tag{6}$$

$$\frac{d\omega}{dt} = -\frac{d\Omega}{dt}\cos i - \frac{1}{he}\left(p\cos\theta a_\mathrm{r} - \left(p+r\right)\sin\theta a_\mathrm{t}\right) \tag{7}$$

$$\frac{dE}{dt} = \frac{na}{r} + \frac{1}{nae}\left(\left[\cos\theta - e\right]a_\mathrm{r} - \left[1+\frac{r}{a}\right]\sin\theta a_\mathrm{t}\right) \tag{8}$$

Where $p = a\left(1-e^2\right)$, $\sqrt{GM_\mathrm{e}p}$, $n = \sqrt{GM_\mathrm{e}a^{-3}}$, $r = p/(1+e\cos\theta)$ and E is the eccentric anomaly. In the equations above $a_{\mathrm{r,t,n}}$ correspond respectively to perturbing acceleration radial, transversal and normal (i.e. perpendicular) to the orbital plane.

3.1.2 Perturbation sources

The following perturbations are considered in the trajectory calculation. The moon is a constraint for the trajectory calculation. The equations and methods are described in detail in another publication [5].

- Oblateness of the Earth
- Atmospheric drag

3.2 Low thrust acceleration

The propulsion system induces the following accelerations:

$$a_{\mathrm{r,thrust}} = \frac{F}{m}\sin\alpha\cos\beta \tag{9}$$

$$a_{\mathrm{t,thrust}} = \frac{F}{m}\cos\alpha\cos\beta \tag{10}$$

$$a_{\mathrm{n,thrust}} = \frac{F}{m}\sin\beta \tag{11}$$

With the pitch (in-plane) angle α and the yaw (out off-plane) angle β and the thrust F provided by the selected propulsion system. The fuel consumed by the propulsion system is computed in the case of an electric engine by:

$$\frac{dm}{dt} = -\frac{2\eta P}{\left(gI_{\mathrm{sp}}\right)^2} \tag{12}$$

Where η is efficiency, P the required power of the system, $g = 9.80665\,\mathrm{m/s^2}$ the gravitational acceleration on the surface of the Earth, and I_{sp} the specific impulse of the system (cf. table 1). In order to track the fuel consumption, equation (12) is added to the set of differential equation given in equations (3) - (7).

3.2.1 Shadow phases

Since a solar powered electric propulsion system is used, possible eclipsing phases are taken into account. Within the simulation it is not distinguished between umbra and penumbra (i.e. penumbra is treated as umbra). Since the system does not provide thrust during the eclipses, the positions where the satellite enters and leaves the shadow of the Earth, have to be known. The entry and exit positions depend on the position of the satellite relative to the Sun and to the Earth. Assuming a conical shadow geometry, the shadow function can be written as:

$$s_c = \frac{\vec{r}_{\mathrm{sat}} \cdot \vec{r}_{\mathrm{sun}}}{r_{\mathrm{sun}}} + \cos\beta\left[\sqrt{r_{\mathrm{sat}} - R_e^2\cos\beta^2} - R_e\sin\beta\right] \tag{13}$$

Where $\vec{r}_{\mathrm{sat,sun}}$ is the position vector of the satellite and the Sun in the geo-centric coordinate system respectively, and $\beta = \arctan\left(R_e + R_s\right) / \left|\vec{r}_{\mathrm{sat}} - \vec{r}_{\mathrm{sun}}\right|$ with R_s the radius of the Sun. If $s_c \leq 0$ the satellite is within the shadow. Given the orbital elements of the satellite together with the starting date, the shadow entry and exit position can be computed.

3.3 Orbital averaging technique

The technique of orbital averaging is used to accelerate the calculations. Therefore, the set of differential equations given in equations (3) - (7) and (12) are re-written in terms of the eccentric anomaly E, using $dE/dt \sim na/r$, assuming that the second term in equation (8) can be neglected. This leads to a new set of differential equations:

$$\frac{da}{dE} = \frac{2a^3}{GM_e}\left(e\sin E a_{\mathrm{r}} + \sqrt{1-e^2}a_{\mathrm{t}}\right) \tag{14}$$

$$\frac{de}{dE} = \frac{a^2}{GM_e}\left[\sin E\left(1-e^2\right)a_{\mathrm{r}} + \left(2\cos E - e - e\cos^2(E)\right)\sqrt{(1-e^2)}a_{\mathrm{t}}\right] \tag{15}$$

$$\frac{di}{dE} = \frac{a^2}{GM_e}\left[\frac{\cos\omega\cos E - e\cos\omega}{\sqrt{1-e^2}} - \sin\omega\sin E\right](1 - e\cos E)\,a_{\mathrm{n}} \tag{16}$$

$$\frac{d\Omega}{dE} = \frac{a^2}{GM_e}\left[\frac{\sin\omega\cos E - e\sin\omega}{\sqrt{1-e^2}} + \cos\omega\sin E\right]\frac{1-e\cos E}{\sin i}a_{\mathrm{n}} \tag{17}$$

$$\frac{d\omega}{dE} = -\cos i\frac{d\Omega}{dE} - \frac{a^2}{eGM_e}\left[(\cos E - e)\sqrt{1-e^2}a_{\mathrm{r}} + \left(2 - e^2 - e\cos E\right)\sin(E)a_{\mathrm{t}}\right] \tag{18}$$

$$\frac{dm}{dE} = -\frac{2\eta P}{\left(gI_{\mathrm{sp}}\right)^2}\frac{r}{na} \tag{19}$$

The equations above are integrated for one orbit, i.e. $-\pi \leq E \leq \pi$ or adequate integration boundaries, taking the eclipsing phases into account. The mean changes in the orbital elements during one revolution can be computed as:

$$\dot{\vec{x}} = \frac{1}{T_p}\int_{E_1}^{E_2}\frac{d\vec{x}}{dE}dE \tag{20}$$

Where $\vec{x} = [a, e, i, \Omega, \omega, m]^T$ is the state vector and $T_p = 2\pi a^{3/2}/\sqrt{GM_e}$ is the orbital period and $E_{1,2}$ are the lower and upper integration boundaries respectively. As long as the difference between orbital averaged and time integrated changes in the orbital elements are small, the averaged changes can be propagated in time. In order to increase the accuracy of the calculations, an adaptive time step depending on the orbital period (between one and ten orbital rotations), is included before the average changes in the orbital elements are updated, using equations (14) to (19) together with an updated state vector.

3.4 Van-Allen radiation belt

Modeling of the radiation belt is based on NASA's AP8 and AE8 models [9], for proton and electron densities in the radiation belts. The models list the spatial distribution of protons with an energy of 100 keV to 400 MeV and electrons with an energy of 40 keV to 7 MeV. The highly energetic particles of the radiation belt will reduce the efficiency of solar panels during their passage through the radiation belts. The degradation depends on the impacting particle type and energy. Typically solar panels are characterized by the manufacturers in terms of degradation due to 1 MeV electrons. The effect of the protons is therefore calculated by a ratio C_{pe}, which relates the impact damage to 1 MeV electron equivalents. The total equivalent electron flux is calculated by:

$$\phi_{1\mathrm{MeV,\,e}} = \int \frac{d\phi_{\mathrm{e}}(E_{\mathrm{e}})}{dE_{\mathrm{e}}} RDC(E_{\mathrm{e}},\, t) dE_{\mathrm{e}} + C_{\mathrm{pe}} \int \frac{d\phi_{\mathrm{p}}(E_{\mathrm{p}})}{dE_{\mathrm{p}}} RDC(E_{\mathrm{p}},\, t) dE_{\mathrm{p}} \tag{21}$$

Where $d\phi_{\mathrm{e}}(E_{\mathrm{e}})$ is the particle flux per energy bin and $\mathrm{RDC}\,(E_{\mathrm{e}},\, t)$ is the relative damage coefficient, which depends on the thickness of the cover glass. Figure 1 shows the calculated equivalent electron flux distribution in the radiation belts [11].

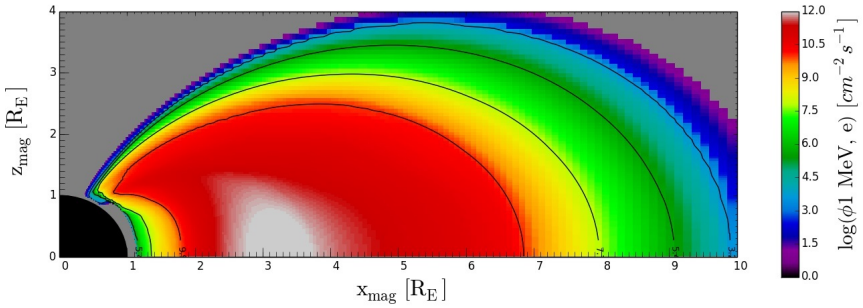

Figure 1: Equivalent 1 MeV electron flux, for XTJ solar cells without cover glass, mapped at normalized distance from the Earth (Earth radii)

In order to reduce degradation of the solar panels a glass cover is applied, which blocks most of the particle impact and protects the solar panels. Figure 2 shows the reduced equivalent electron flux due to glass cover of the solar panels. Both figures use the same color scale for comparison. A glass coating of a thickness of $s = 0.335$ mm reduces the equivalent electron flux from up to $\phi_{1\mathrm{MeV,\,e}} = 10^{12.2}$ $\mathrm{cm^{-2}s^{-1}}$, to a moderate maximum of $\phi_{1\mathrm{MeV,\,e}} = 10^{7.4}$ $\mathrm{cm^{-2}s^{-1}}$.

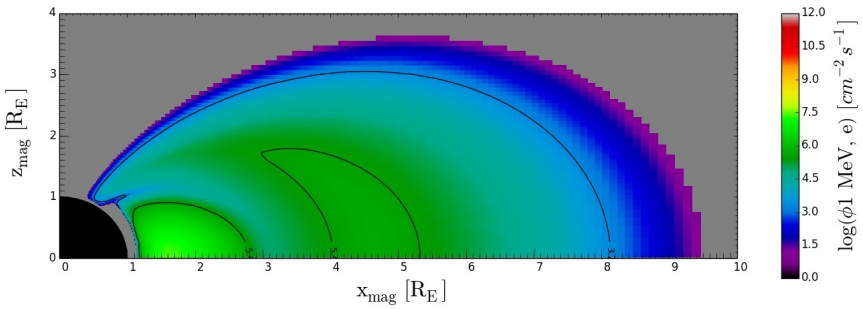

Figure 2: Equivalent 1 MeV electron flux, for XTJ solar cells with cover glass of $s = 0.335$ mm thickness, mapped at normalized distance from the Earth (Earth radii)

The equivalent 1MeV electron flux is included as an additional equation in the set of differential equations (14) - (19) and is integrated along the orbit of the satellite by:

$$\frac{d\phi_{1\mathrm{MeV,\,e}}}{dE} = \phi_{1\mathrm{MeV,\,e}} \frac{r}{na} \tag{22}$$

3.5 Steering laws and trajectory optimization

For the direct optimization approach, the thrust steering direction is parameterized. The thrust steering direction is given by:

$$\vec{u} = [\sin\alpha\cos\beta, \cos\alpha\cos\beta, \sin\beta]^T \tag{23}$$

See also equations (9) to (11). It is characterized by the pitch α and the yaw β steering angles. A Hamiltonian function is defined (as discussed in text book literature [3]):

$$\mathcal{H}\left(\vec{x}, \vec{u}, \vec{\lambda}\right) = \lambda_a \frac{da}{dE} + \lambda_e \frac{de}{dE} + \lambda_i \frac{di}{dE} \tag{24}$$

With costate variables $\vec{\lambda} = [\lambda_a, \lambda_e, \lambda_i]^T$. The pitch and yaw steering laws can be obtained from the Hamiltonian function by computing its derivation with respect to α ($\partial\mathcal{H}/\partial\alpha$) and β ($\partial\mathcal{H}/\partial\beta$). Following textbook [3] literature, it is meaningful to parameterize the costate variables along the semi-major axis by several grid points and performing a linear interpolation between them. The optimization searches for the optimal steering law, which minimizes the selected performance index J, which is subject to the equations of motion, $\dot{\vec{x}} = f(t, \vec{x}, \vec{u})$, i.e. the variation in the orbital elements due to several perturbations, and to the final state constraints $\psi\left[\vec{x}\left(t_f\right), t_f\right]$. For this purpose a parallel Lagrange multiplier particle swarm optimizer [7] is used.

3.6 Numerical technique

The method is based on the one described by Yang [13]. The Earth-moon trajectory is split in this study into two parts:

(i). low Earth orbit (LEO) to high Earth orbit (HEO)

(ii). HEO to high lunar orbit (HLO)

HEO is here defined as an elliptical orbit with a semi major axis of $a \sim 11\ R_e$, with respect to the Earth radius R_e = 6370 km. Typical low-thrust trajectories imply several hundreds to thousands of rotations around the central body, which leads to huge computational demands during the integration of the differential equations. Therefore, the orbital averaging technique is applied to the first part of the trajectory. The second part of the trajectory includes only a few tens of rotations around the Earth and is therefore integrated in time.

4. Case study

In this section a reference launcher is selected, for which resulting lunar payloads, depending on the initial orbits are analyzed.

4.1 Launcher options

As initially stated, the premise of the discussed mission is to be a low cost technology demonstrator. Table 5 lists different commercially available launchers and their official cost. For cost in US$ an exchange rate of 1.1 to the Euro (€) is assumed. Performance data of *Falcon 1* is listed, although the launcher is out of operation. Similar micro launchers, which are currently in planning or under development, aim at achieving launch prices around 5 M€. Falcon 1 can therefore be considered conservative in terms of cost.

Table 5: Commonly used commercially available launchers

	Falcon 1[a]	**VEGA**	**Falcon 9 v1.1**	**Ariane 5 ES**	**Proton-M**
Orbital payload	200 kg	1500 kg	13150 kg	20700 kg	21600 kg
Perigee	650 km	700 km	200 km	260 km	200 km
Apogee	700 km	700 km	200 km	260 km	200 km
Inclination	28.5°	90°	28.5°	5.4°	51.6°
Launch cost	7.3 M€	32 M€	55.6 M€	150 M€	91 M€
Specific cost	36400 €/kg	21300 €/kg	4230 €/kg	7250 €/kg	4200 €/kg

[a] Launcher out of service

For this study *VEGA* is selected as reference launcher. This is due to the moderate specific cost, as well as the low total cost.

4.1.1 Launcher orbital payload performance

While the reference orbit of *VEGA* is listed in table 5, different orbits can be reached by this launcher. Figure 3 shows the payload performance in different orbital altitudes and inclinations [10].

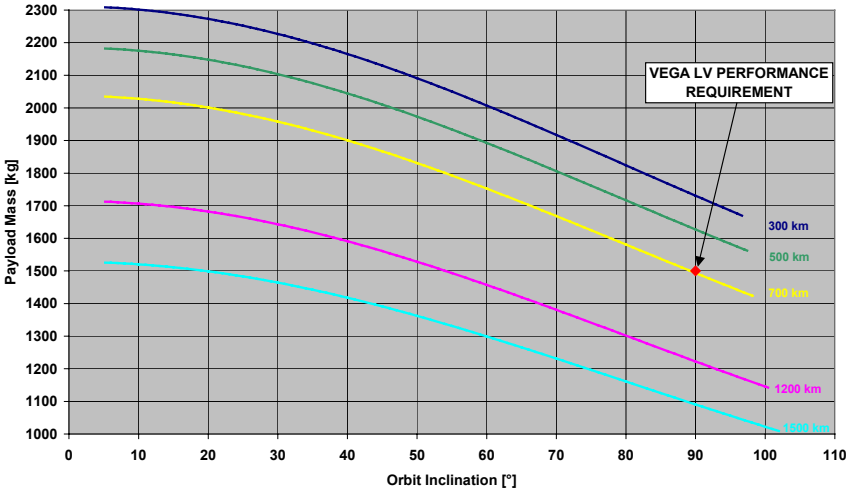

Figure 3: Vega payload performance in different orbits [10]

Direct insertion in lunar transfer orbit (LTO) is not considered an option in this study, as the low specific impulse of the launcher's propulsion, compared with electrical propulsion results in much less lunar payload mass.

4.2 Performance calculation

Table 6 lists the results of the performed trajectory calculations. The flight time is optimized. Depending on the accuracy of the achieved final lunar orbit, within the predefined boundaries, the required propellant mass (which is not optimized in this calculation) differs. The required Δv and propellant mass is largely depended on the initial orbit conditions. Table 7 lists the averaged final masses, required propellant masses and Δv for the different initial orbits. As can be noted, due to the non Hohmann type transfers, used with SEP, the required Δv are substantially higher than those required for high thrust propulsion (listed as *ideal* Δv for comparison in table 7). Due to the large specific impulse, SEP is however still much more efficient than conventional propulsion.

As a reference case the initial orbit of 300 km at an inclination of 20 degrees, with two thrusters is selected. Figure 4 shows the optimizer results for the trajectory, between LEO and HLO, for this selected reference case. The trajectory between HEO and HLO is shown in a 3D plot in figure 5.

As can be seen in table 7 a starting altitude of 300 km results in the highest final masses. At that altitude the atmospheric drag is already negligibly small. At high starting altitude the initial orbital mass is significantly reduced, reducing the achievable final mass. The starting orbit has a little impact on the integrated particle flux. It is possible to minimize the particle flux by starting at high altitudes and using high thrust levels. The radiation levels of the considered trajectories will cause performance losses of 10% or less. The number of thrusters has obviously a strong impact on the required flight time. One has however to consider, that the achievable payload mass is significantly reduced, the more thrusters are used. Due to the required power, mass and cost of power related components, most notably the solar panels, increases with the number of thrusters.

For comparison the nominal *VEGA* trajectory, as listed in table 5, with 1500 kg payload in sun synchronous orbit (SSO), was also analyzed as a starting point. This trajectory is however very badly suited for the purpose of launching a lunar transfer vehicle. This is on the one hand because the 700 km orbital altitude is already comparatively high and on the other hand the inclination, required for the polar SSO, has to be reduced again by the satellite, to reach the moon.

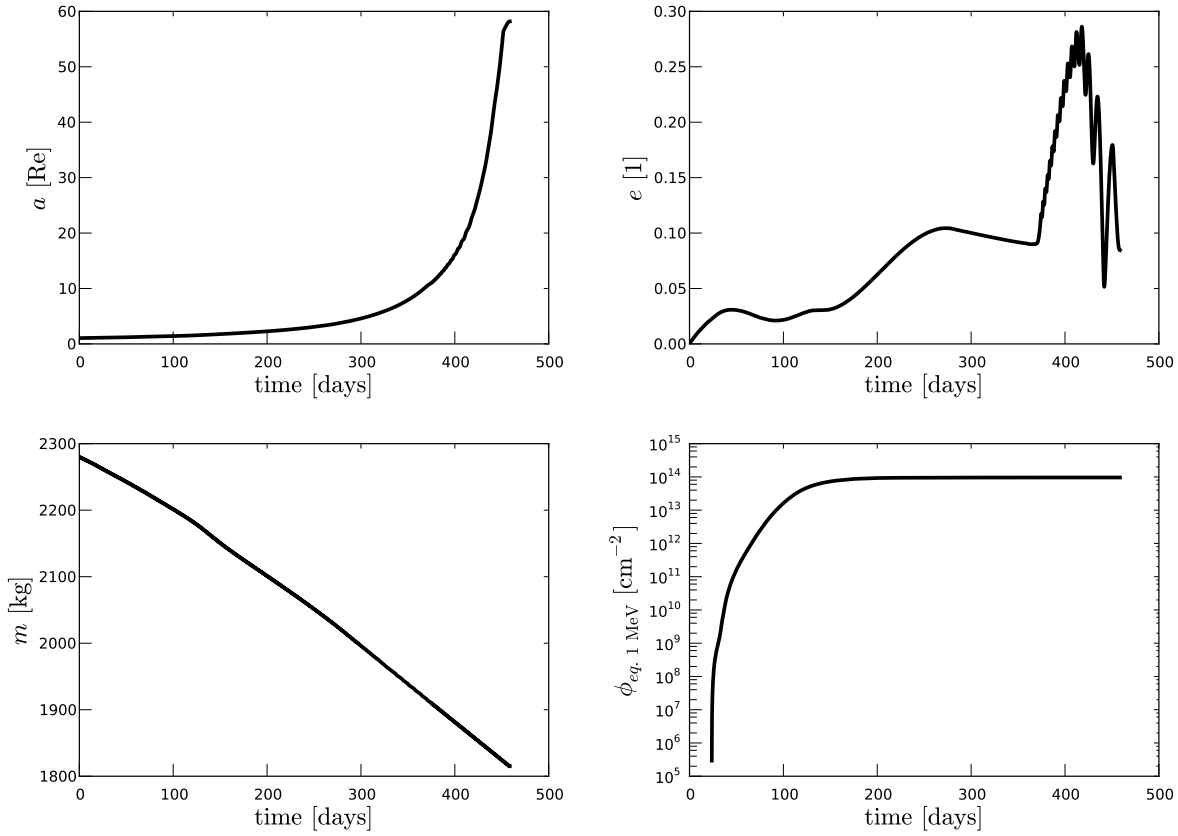

Figure 4: Trajectory optimization results for the transfer between LEO and HLO

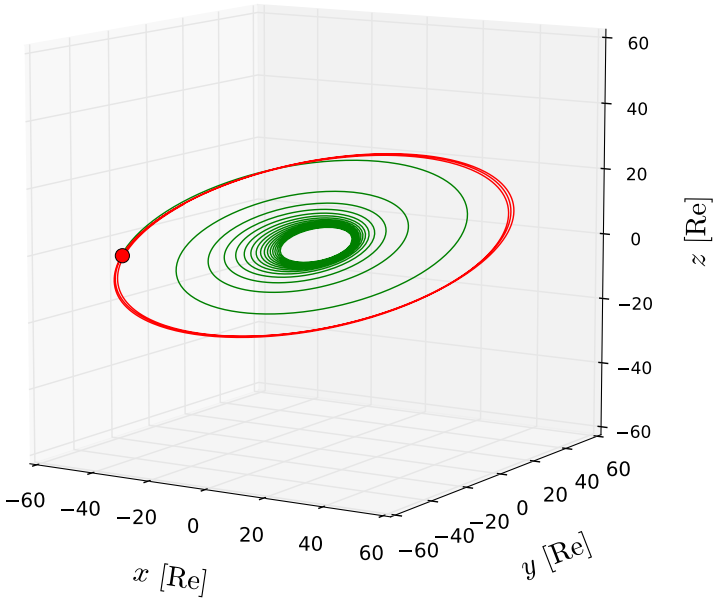

Figure 5: 3D trajectory between HEO and HLO

Table 6: Trajectory calculation results

SEP thrust	initial orbit	initial incl.	initial mass	equiv. el. flux	flight time
0.2 N	300 km	20°	2280 kg	$10^{14.34}$ 1/cm^2	905 d
0.4 N	300 km	20°	2280 kg	$10^{13.98}$ 1/cm^2	459 d
0.6 N	300 km	20°	2280 kg	$10^{13.73}$ 1/cm^2	310 d
0.8 N	300 km	20°	2280 kg	$10^{13.56}$ 1/cm^2	244 d
0.2 N	700 km	20°	2000 kg	$10^{14.24}$ 1/cm^2	756 d
0.4 N	700 km	20°	2000 kg	$10^{13.84}$ 1/cm^2	384 d
0.6 N	700 km	20°	2000 kg	$10^{13.74}$ 1/cm^2	255 d
0.8 N	700 km	20°	2000 kg	$10^{13.78}$ 1/cm^2	189 d
0.2 N	1500 km	20°	1500 kg	$10^{14.04}$ 1/cm^2	534 d
0.4 N	1500 km	20°	1500 kg	$10^{13.97}$ 1/cm^2	265 d
0.6 N	1500 km	20°	1500 kg	$10^{13.65}$ 1/cm^2	180 d
0.8 N	1500 km	20°	1500 kg	$10^{13.45}$ 1/cm^2	134 d
0.2 N	300 km	30°	2250 kg	$10^{14.13}$ 1/cm^2	928 d
0.4 N	300 km	30°	2250 kg	$10^{13.89}$ 1/cm^2	476 d
0.6 N	300 km	30°	2250 kg	$10^{13.54}$ 1/cm^2	324 d
0.8 N	300 km	30°	2250 kg	$10^{13.48}$ 1/cm^2	235 d
0.2 N	700 km	30°	1950 kg	$10^{14.01}$ 1/cm^2	770 d
0.4 N	700 km	30°	1950 kg	$10^{13.68}$ 1/cm^2	378 d
0.6 N	700 km	30°	1950 kg	$10^{13.64}$ 1/cm^2	253 d
0.8 N	700 km	30°	1950 kg	$10^{13.62}$ 1/cm^2	187 d
0.2 N	1500 km	30°	1450 kg	$10^{13.92}$ 1/cm^2	541 d
0.4 N	1500 km	30°	1450 kg	$10^{13.75}$ 1/cm^2	272 d
0.6 N	1500 km	30°	1450 kg	$10^{13.42}$ 1/cm^2	179 d
0.8 N	1500 km	30°	1450 kg	$10^{13.29}$ 1/cm^2	134 d
0.4 N	700 km	89°	1500 kg	$10^{13.48}$ 1/cm^2	456 d

Table 7: Required propellant masses

initial mass	initial orbit	initial incl.	ideal Δv	final mass	propellant	SEP Δv
2280 kg	300 km	20°	3913 m/s	1815 kg	465 kg	9390 m/s
2000 kg	700 km	20°	3814 m/s	1607 kg	393 kg	9020 m/s
1500 kg	1500 km	20°	3637 m/s	1215 kg	285 kg	8670 m/s
2250 kg	300 km	30°	4081 m/s	1763 kg	487 kg	10040 m/s
1950 kg	700 km	30°	3982 m/s	1551 kg	399 kg	9440 m/s
1450 kg	1500 km	30°	3805 m/s	1162 kg	288 kg	9110 m/s
1500 kg	700 km	89°	4903 m/s	1019 kg	482 kg	15950 m/s

4.3 Mission mass analysis

Table 8 shows the mass breakdown for the selected reference case. Many components are discussed in more detail in section 2.1. The masses of structure, thermal control, harness, guidance, navigation and control (GNC), RCS, and communications are based on typical fractions for satellite mass break downs. For the power control and distribution unit (PCDU) a mass of 0.005 kg/W is assumed. It is assumed that system functions, such as communications and GNC, are shared between the in space vehicle listed here and the "payload". Since all individual mass estimations contain explicit or implicit margins, no global margin is added. The global margin, as the sum of the individual component margins, is in this case roughly 10%.

Table 8: Lunar mission mass breakdown

component	mass	fraction
structure	342.0 kg	15.0%
thermal control	114.0 kg	5.0%
RCS	45.6 kg	2.0%
solar panels	128.1 kg	5.6%
PCDU	77.0 kg	3.4%
harness	68.4 kg	3.0%
GNC	68.4 kg	3.0%
communications	91.2 kg	4.0%
propulsion system	17.6 kg	0.8%
valves	7.2 kg	0.3%
tank	81.7 kg	3.6%
propellant	488.8 kg	21.4%
payload*	750.0 kg	32.9%

* a mass breakdown for the payload can be found in section 2

Tables 9 to 10 list the mass breakdown of a possible lander, and sample return vehicle (SRV) respectively, with a total mass of 750 kg. The mass estimation is based on empirical equations found in literature [6, 8]. For the propellant calculation, the Δv of table 4 are used together with an assumed lander propulsion vacuum specific impulse of I_{vac} = 320 s. The mass of 750 kg of the landing vehicle does not allow for a lunar rover.

Table 9: Mass break down of lunar landing vehicle

Component	Mass	Mass percentage
Propellant	355.5 kg	47.4 % of lander mass
Lander vehicle dry mass	394.5 kg	52.6 % of lander mass
Propulsion system	17.8 kg	5 % of lander propellant mass
Tanks	35.6 kg	10 % of lander propellant mass
Propellant reserve	21.3 kg	6 % of lander propellant mass
Valves & pipes	7.5 kg	1 % of lander mass
Power supply	15.0 kg	2 % of lander mass
Structure & landing gear	71.25 kg	9.5 % of lander mass
Thermal control mass	15.0 kg	2 % of lander mass
Onboard computer fraction	7.5 kg	1 % of lander mass
Electrical harness	22.5 kg	3 % of lander mass
GNC	7.5 kg	1 % of lander mass
Scientific instruments	7.5 kg	1 % of lander mass
Communications	7.5 kg	2 % of lander mass
Sample Return Vehicle	158.6 kg	24.6 % of lander mass

4.4 Mission cost breakdown

Figure 6 shows a breakdown of estimated mission cost. The cost of the propellant xenon, based on current market prices of 20 €/l [2] at standard ambient temperature and pressure (SATP), equals to approximately 3500 €/kg. Solar

Table 10: Mass break down of sample return vehicle (SRV)

Component	Mass	Mass percentage
Propellant	100.3 kg	63.2 % of SRV mass
SRV dry mass	58.3 kg	36.8 % of SRV mass
Propulsion system	5.0 kg	5 % of SRV propellant mass
Tanks	10.0 kg	10 % of SRV propellant mass
Propellant reserve	6.0 kg	6 % of SRV propellant mass
Valves & pipes	1.6 kg	1 % of SRV mass
Power supply	3.2 kg	2 % of SRV mass
Structure	11.9 kg	7.5 % of SRV mass
Thermal control mass	3.2 kg	3 % of SRV mass
Onboard computer fraction	1.6 kg	1 % of SRV mass
Electrical harness	4.8 kg	3 % of SRV mass
GNC	1.6 kg	1 % of SRV mass
Communications	3.2 kg	2 % of SRV mass
Sample Return Capsule	6.3 kg	3.8 % of SRV mass

panel cost per power is assumed to be 1000 €/W [1], which results in a specific cost of 120000 €/kg for the solar panels. Mission control cost is assumed to be equivalent to 100 persons working at a price level of 100 k€ per person per year. All remaining component costs, displayed in figure 6, are arbitrarily selected in relation to known cost figures.

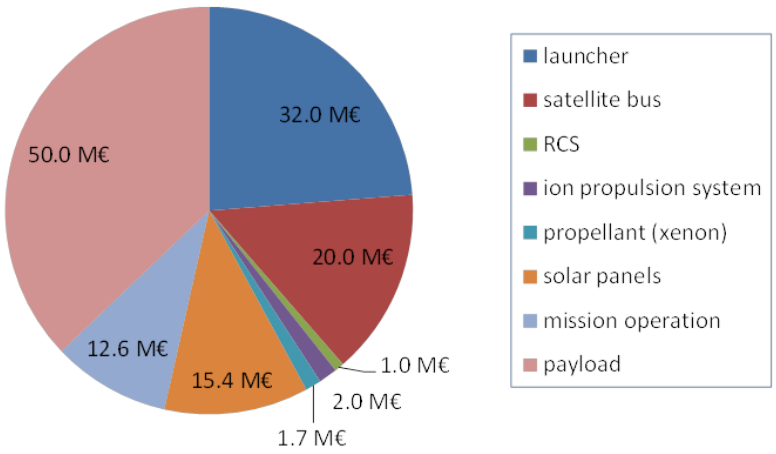

Figure 6: Cost estimation overview

5. Conclusion and Outlook

Sample trajectories for solar electric propulsion transfer from low Earth orbit to high lunar orbit were analyzed. The selected launcher for this case study was the European *VEGA* launcher. Different starting orbits and number of thrusters were considered. The highest mass of lunar orbital payload, of the considered cases, was reached with a single thruster, starting from 300 km initial orbital altitude at an initial orbital inclination of $i = 20°$. Since the flight duration and the associated passage time through the radiation belts is very long in this case, due to the unfavorable thrust to mass ratio, the suggested approach is to use two thrusters. In this case the transfer time amounts to 459 days, with an initial vehicle mass of 2280 kg and a thrust of 0.4 N. Propellant consumption, including reserves, is 488.8 kg of xenon, which amount to 1.3 % of the total expected mission cost of 135 M€. The discussed mission seems feasible within European research & technology budgets.

Further studies will include any or all of the following additional aspects. Further studies may include a space debris impact risk model. Additional perturbations by the sun's gravitation and solar pressure may be included in the model. Optimization may be performed with regards to passage time through the radiation belts and associated failure

risks. Alternative optimization may minimize fuel consumption in order to maximize the payload mass. Different launcher options, including heavy launchers and small launchers, as well as piggy back and dual launch options may be analyzed. Different propulsion options for the in-space propulsion, as well as for the lander vehicle may be considered. Trajectories starting from lower orbits (e.g. 200 km low Earth orbit) may be considered, to find an optimum starting orbit.

References

[1] Bailey, S., and Raffaelle, R. Space Solar Cells and Arrays. In *Handbook of Photovoltaic Science and Engineering*, A. Luque and S. Hegedus, Eds. Wiley, July 2003, ch. 10, pp. 413–448.

[2] Betzendahl, R. The Rare Gases Market Recovers with Global Economies. *CryoGas International 49*, 03 (Mar. 2011), 40–43.

[3] Conway, B. A. *Spacecraft Trajectory Optimization*. Cambridge University Press, New York, NY, 2014.

[4] Ellerbrock, H. *Orbital Propulsion Fluidic Equipment*. Airbus Defence & Space, Munich, Germany, 2013. [Online; accessed 2015-06-02] `http://cs.astrium.eads.net/sp/spacecraft-propulsion/valves/index.html`.

[5] Fromm, C. M. Using electric propulsion for the de-orbiting of satellites. In *5th CEAS Air & Space Conference* (Delft, The Netherlands, Sept. 2015).

[6] Heineman, Jr., W. Mass Estimating and Forecasting for Aerospace Vehicles Based on Historical Data. Tech. Rep. JSC-26098, NASA, Houston, TX, Nov. 1994.

[7] Jansen, P., and Perez, R. Constrained structural design optimization via a parallel augmented lagrangian particle swarm optimization. *Journal of Computers and Structures 89* (July 2011), 1352–1366.

[8] Messerschmid, E., and Fasoulas, S. *Raumfahrtsysteme: Eine Einführung mit Übungen und Lösungen*, 4 ed. Springer, Oct. 2010.

[9] National Space Science Data Center. *NASA Radiation Belt Models AP-8 and AE-8*. Washington, D.C., 1980.

[10] Perez, E. *VEGA User's Manual*, 3 ed. Arianespace, Evry, France, Mar. 2006. [Online; accessed 2015-06-02] `http://www.arianespace.com/launch-services-vega/VEGAUsersManual.pdf`.

[11] Schubert, F. Analyse Elektrischer Antriebssysteme als Ersatz für Konventionelle Oberstufen. Tech. Rep. V01, Deutsches Zentrum für Luft- und Raumfahrt e.V. (DLR), Lampoldshausen, Germany, Oct. 2014. DLR-LA-RAS-RP-009.

[12] Spectrolab, Inc. *29.5% NeXt Triple Junction (XTJ) Solar Cells*. Sylmar, CA, Sept. 2012. [Online; accessed 2015-06-03] `http://www.spectrolab.com/solarcells.htm`.

[13] Yang, G. Earth-moon Trajectory Optimization Using Solar Electric Propulsion. *Chinese Journal of Aeronautics 20*, 5 (Oct. 2007), 452–468.